Sol–gel derived $Ba/SrTiO_3$–MgF_2 solar control coating stack on glass for architectural and automobile applications

R. Subasri, D. S. Reddy, K. R. C. Soma Raju, K. S. Rao, P. Kholov & N. Gaponenko

Research on Chemical Intermediates

ISSN 0922-6168
Volume 45
Number 8

Res Chem Intermed (2019)
45:4179-4191
DOI 10.1007/s11164-019-03899-w

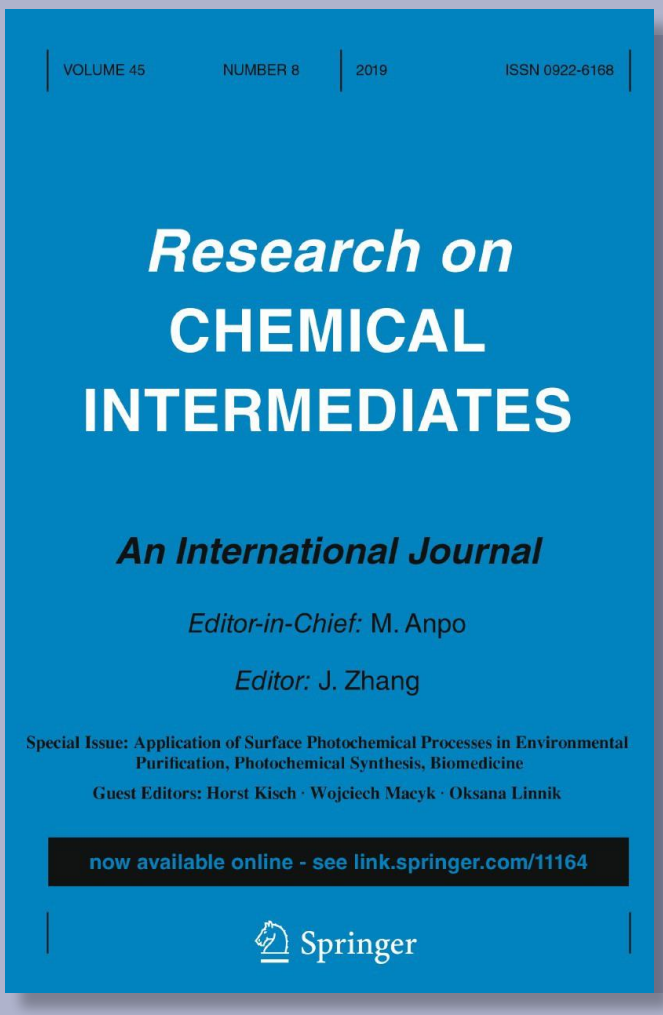

Research on Chemical Intermediates (2019) 45:4179–4191
https://doi.org/10.1007/s11164-019-03899-w

Sol–gel derived $Ba/SrTiO_3$–MgF_2 solar control coating stack on glass for architectural and automobile applications

R. Subasri[1] · D. S. Reddy[1] · K. R. C. Soma Raju[1] · K. S. Rao[1] · P. Kholov[2] · N. Gaponenko[2]

Received: 10 January 2019 / Accepted: 8 April 2019 / Published online: 27 June 2019

Abstract
Fully dielectric solar control coatings based on alternating layers of Ba (or Sr) TiO_3 and MgF_2 were deposited on soda lime glass substrates. Three-layered stacks $BaTiO_3/MgF_2/BaTiO_3$ and $SrTiO_3/MgF_2/SrTiO_3$ were generated using $BaTiO_3$, $SrTiO_3$ and MgF_2 sols deposited on glass using dip coating technique. The multi-layered coating stack was fired at 450 °C with different heating rates using a conventional muffle furnace and a conveyorized belt furnace, by which two methods of heat treatment were investigated. Heat treatment after deposition of each layer and a consolidated firing of the three-layered stack with intermediate drying between the layers were carried out and optical properties of the coatings compared. The heat treated coatings were characterized for their UV–Vis–NIR transmittance, microstructure, phase purity, thickness and refractive indices. The coating stack based on $BaTiO_3$ as the high refractive index material in conjunction with MgF_2 exhibited better solar control properties than $SrTiO_3$ as the high refractive index material. Moreover, a fast firing of the $BaTiO_3/MgF_2/BaTiO_3$ stack in a conveyorized belt furnace yielded good NIR blocking and solar control properties, whereas slow firing in a muffle furnace exhibited ~ 80% visible light transmittance with an NIR transmittance of ~ 75%.

Keywords Solar control coatings · NIR transmittance · Sol–gel · Glass · Automotive · Architectural

* N. Gaponenko
nik@nano.bsuir.edu.by

R. Subasri
subasri@arci.res.in

[1] Centre for Sol-Gel Coatings, International Advanced Research Centre for Powder Metallurgy and New Materials (ARCI), Balapur, Hyderabad, Telangana State 500 005, India

[2] Laboratory of Nanophotonics, Belarusian State University of Informatics and Radioelectronics (BSUIR), P. Browka 6, 220013 Minsk, Belarus

Introduction

Glass, which is used in buildings and automobiles is highly transparent to both visible and near infrared (NIR) radiation; the Vis–NIR transmittance being ~90%. This is a cause for serious concern, more so in tropical countries, since due to the high NIR transmittance, the load on air conditioners in an automobile or inside a building increases. In this context, there are concerted efforts to make the glass more energy efficient so as to reduce the NIR transmittance without compromising much on the visible light transmittance. Polymer-based solar control films are usually stuck onto the glass windows in automobiles or high rise buildings to block the NIR radiation. However, the drawback with these polymer films is that they have very short durability due to their reactivity with UV radiation in addition to possessing poor mechanical properties like scratch resistance, etc., and hence, need to be replaced quite often. IR reflective coatings based on metal dielectric stacks need to be protected from the environment due to softness and reactivity of the metallic layers to oxygen and humidity. In addition, they are cost-intensive. Transparent conducting oxide (TCO) films based on indium tin oxide have also been investigated as suitable alternates to the polymer-based sun control films and metal-dielectric based IR reflective coatings on glass [1, 2]. Nevertheless, due to depleting reserves of indium, these TCO based solar control coatings are no longer preferred by the industry and require replacement. Interested readers may refer to a recent review by V. A. Maiorov on Window Glasses: State and Prospects [3]. A cost-effective substitute would be to design a fully dielectric system, consisting of multilayer stacks of alternate high and low refractive index materials of quarter wavelength thickness, so as to produce a dielectric reflector that can reflect radiation in the near-infrared region, while maintaining a high visible light transmittance. Moreover, fully dielectric coatings might be expected to have better mechanical properties like scratch and abrasion resistance when compared to polymer based sun control films or metal-dielectric systems. There are very few reports on the use of a fully dielectric system on glass for solar control applications and previous studies on this topic also focused on use of only TiO_2 as high refractive index layer and silica/porous silica (zeolite) as low refractive index material [4–6]. Ba/$SrTiO_3$ has been explored more as a dielectric material for capacitor applications [7–9] and as a photocatalyst for environmental detoxification and energy production [10–14]. However, as materials possessing high refractive index, they remain less investigated for optical applications and so far, use of $BaTiO_3$ or $SrTiO_3$ has not been explored as high refractive index material for generating solar control coatings on glass. Hence, the objective of the present study was to investigate for the first time in the literature, the feasibility of using $BaTiO_3$ and $SrTiO_3$ as high refractive index materials and MgF_2 as the low refractive index material, to generate a fully dielectric solar control coating stack. Multilayer coating stacks with the configurations $BaTiO_3$ (or $SrTiO_3$)/MgF_2/|$BaTiO_3$ (or $SrTiO_3$) were generated by dip coating technique on soda lime glass substrates and characterized for their solar control properties. The optical properties like Vis–NIR transmittance, refractive index and thickness were

measured along with the analysis of their microstructures. The optical properties were compared and evaluated for their possible applications in automotive and architectural sectors.

Experimental

Materials

Barium acetate (99% purity, SRL), Strontium acetate (99% purity, Sigma Aldrich), acetic acid (SD Fine Chemicals), titanium isopropoxide (ABCR), acetyl acetone (extra pure SRL), magnesium acetate (extra pure SRL), and HF (SD Fine Chemicals) were used as starting materials without further purification. Commercially available soda lime glass (SLG) coupons of dimensions 7.5 cm × 2.5 cm × 0.3 cm were used as substrates.

Sol synthesis, coating deposition and heat treatment

$BaTiO_3$ and $SrTiO_3$ sols were synthesized using a 1:1 mol ratio of barium acetate/strontium acetate and titanium isopropoxide. MgF_2 sol was synthesized using the procedure as mentioned elsewhere [15]. Coatings were deposited using dip coating technique by employing different withdrawal speeds, ranging from 0.5 to 6 mm/s for each layer. Initially, each layer was heat treated at 450 °C before deposition of the subsequent layer using a muffle furnace. A conventional muffle furnace (Nabertherm GmbH, Germany) where the total cycle time was 330 min (heating rate of 1 °C/min with a soaking time of 60 min @ 450 °C) and a conveyorized belt furnace (Linn Hightherm GmbH, Germany) with total cycle time of only 30 min (with a soaking time of 10 min at 450 °C) per layer were employed to study the effect of different heat treatment schedules on the morphology, phase composition and optical properties. In some cases, only drying at 100 °C between the layers was carried out and a final heat treatment at 450 °C was carried out after deposition of all three layers.

Characterization

Phase composition of heat treated powders and coatings was studied using an X-ray diffractometer, model Bruker Axs D8 Advance. The coating thickness and refractive index of the individual layers were determined using ellipsometric data acquired by a variable angle spectroscopic ellipsometer (J.A. Wollam Inc., USA). The ellipsometric data were analyzed using a standard Cauchy model. The surface morphology and elemental analysis of the coated SLG substrates were studied using a scanning electron microscope (SEM, model Hitachi S-4800). The transmittance of the coatings was measured using a SHIMADZU make UV-3600 plus model UV–Vis–NIR Spectrophotometer. Adhesion strength of the coatings to substrate was evaluated as per ASTM D 3359-17.

Results and discussion

The UV–Vis–NIR transmittance spectra for the single layered coatings after deposition of $BaTiO_3$, $SrTiO_3$ and MgF_2 using different withdrawal speeds are given in Figs. 1, 2 and 3.

The average percentage transmittance evaluated from the transmittance data for the visible and NIR wavelength ranges are presented in Table 1.

Coating thickness of $BaTiO_3$, MgF_2 and $SrTiO_3$ layers for the three-layered coating stack was selected based on the spectral transmittance of the respective single layer coatings applied on individual soda lime glass substrate and heat treated in a batch furnace as presented in Figs. 1, 2, 3 and Table 1, respectively. Accordingly, the withdrawal speed that yielded the maximum visible light transmittance and minimum NIR transmittance was chosen as optimum coating parameter, which is bold faced in Table 1. In the case of $BaTiO_3$ and $SrTiO_3$, it was 2 mm/s and in the case of MgF_2, it was 3 mm/s.

Single layered $BaTiO_3$, MgF_2 and $SrTiO_3$ coatings that were selected for depositing required stacks and generated with optimized withdrawal speeds were also subjected to variable angle spectroscopic ellipsometric analysis, for thickness and

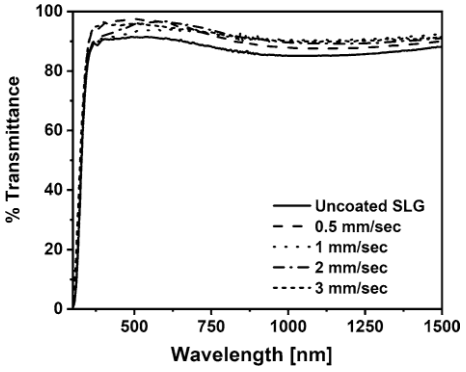

Fig. 1 Transmittance spectra of MgF_2 on SLG

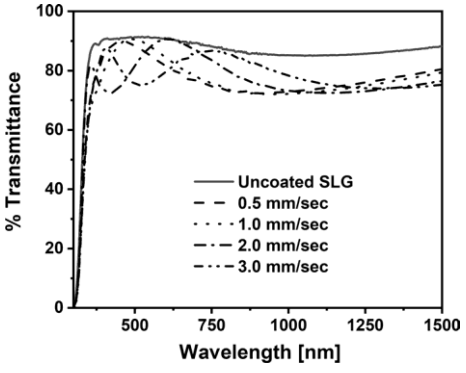

Fig. 2 Transmittance spectra of $BaTiO_3$ on SLG

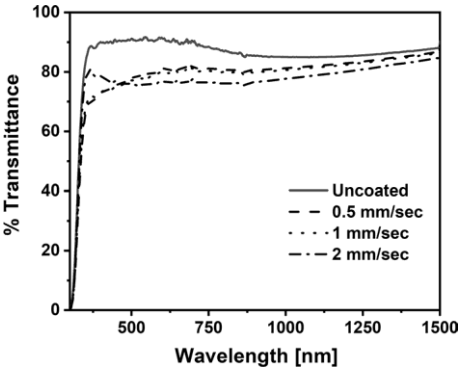

Fig. 3 Transmittance spectra of $SrTiO_3$ on SLG

refractive index measurements. The results of the spectroscopic ellipsometric analysis are shown in Figs. 4, 5 and 6.

Cauchy model fitting was employed to fit the ellipsometry data and their coating thickness and refractive index values obtained after analysis are presented in Table 2.

The three-layered stacks with configuration $BaTiO_3/MgF_2/BaTiO_3$ and $SrTiO_3/MgF_2/SrTiO_3$ were generated and Vis–NIR transmittance measured. The adhesion of the three-layered coating stack measured as per ASTM-D3359-17 was found to be of rank 5B (no coating removal after removal of the tape). The elemental analysis of the three-layer coated SLG substrates showed the presence of barium, titanium, magnesium, fluorine and oxygen elements in the first stack and strontium, titanium, magnesium, fluorine and oxygen elements in the second stack as seen from Fig. 7. This confirmed the composition of the respective coating stacks. Presence of silicon and calcium peaks in the spectra of both coating stacks are from the substrate.

XRD analysis of $BaTiO_3$ and $SrTiO_3$ coatings on glass showed that the films were X-ray amorphous, since the temperature of 450 °C was not sufficient to cause their crystallization. MgF_2 powders obtained by drying of the MgF_2 sol when subjected to XRD analysis showed good crystallinity, as shown in Fig. 8 and matched with the ICDD file 01-070-8281.

The transmittance spectra for the three-layered coatings stacks (a) $BaTiO_3/MgF_2/BaTiO_3$ and (b) $SrTiO_3/MgF_2/SrTiO_3$ are shown in Fig. 9a, b respectively and average values of transmittance obtained from the transmittance spectra are presented in Table 3.

Even though, the $BaTiO_3$-based stack has exhibited reduced transmittance as compared to $SrTiO_3$ based stack in the visible wavelength range, its transmittance in the NIR range has been reduced to a large extent. A good solar control coating must exhibit high visible light transmittance with a low NIR transmittance. Though the visible wavelength transmittance in the $BaTiO_3$-based stack was lower than the $SrTiO_3$-based stack, the values were still quite close to the minimum required transmittance value of 70% for commercial applications. Based on this, it was concluded that $BaTiO_3$ in conjunction with MgF_2 was yielding better solar control properties

Table 1 Transmittance data of individual layers heat treated in conventional muffle furnace

SLG sample with coating generated at different deposition rate	Transmittance % at corresponding wave length range (nm)							
	0.5 mm/s speed		1.0 mm/s speed		2.0 mm/s speed		3.0 mm/s speed	
	400–800	800–1500	400–800	800–1500	400–800	800–1500	400–800	800–1500
$BaTiO_3$	81.8	75.2	83.1	74.4	*83.8*	*74.3*	81.9	77.0
$SrTiO_3$	81.0	86.3	80.6	86.0	*80.2*	*84.1*	–	–
MgF_2	93.6	90.3	93.3	90.0	94.2	90.2	*94.5*	*90.5*

The optimized withdrawal speeds for which visible light transmittance is highest and NIR transmittance is lowest has been bold faced and italicized

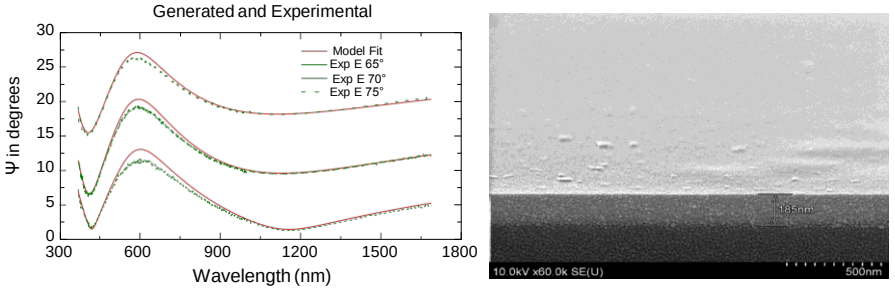

Fig. 4 Ellipsometer thickness profile of $BaTiO_3$ coating and the corresponding SEM image of the cross-section, thickness: 188.0 nm

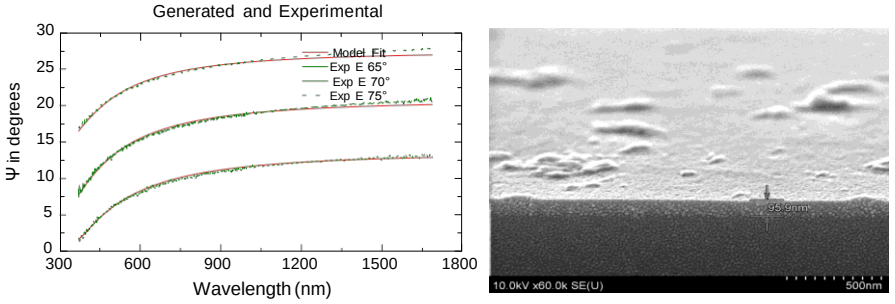

Fig. 5 Ellipsometer thickness profile of $SrTiO_3$ coating and the corresponding SEM image of the cross-section, thickness: 96.0 nm

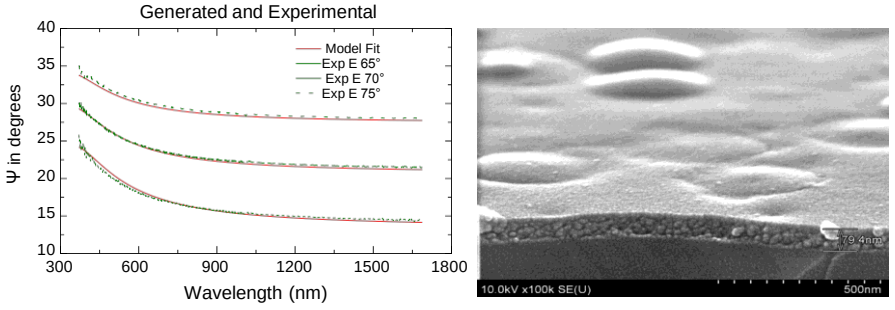

Fig. 6 Ellipsometer thickness profile of MgF_2 coating and the corresponding SEM image of the cross-section, thickness: 71.4 nm

than $SrTiO_3$ and hence, for further experiments, only $BaTiO_3$ was used as the high refractive index material.

Further experiments were conducted to reduce the heat treatment cycle time of $BaTiO_3/MgF_2/BaTiO_3$ stack while keeping the soaking temperature unaltered at 450 °C and reducing the ramp up and down time using a belt furnace. The spectral

Table 2 Refractive index values of single layer $BaTiO_3$, MgF_2 and $SrTiO_3$ heat treated in batch furnace

SLG sample with coating	Refractive index (n) at			Thickness (nm)
	550	800	1300	
$BaTiO_3$	1.85	1.81	1.78	188.0
MgF_2	1.38	1.38	1.38	71.4
$SrTiO_3$	1.70	1.65	1.62	96.0

transmittance spectra obtained from samples with different heat treatment schedules are depicted in Fig. 10 and the corresponding average transmittance values in visible and NIR range are presented in Table 4.

From Fig. 10, it is clearly evident that the lowest NIR transmittance, i.e., highest NIR reflectance was found to be at a longer wave length 1000 nm for belt furnace heat treated sample as against batch furnace heat treated sample that showed maximum NIR blocking at 850 nm for the same coating stack material applied at the identical coating conditions.

Analysis of the three-layered coating stack with respect to thickness and refractive index was carried out using spectroscopic ellipsometric data as shown in Fig. 11.

Cauchy model was used to fit the ellipsometric data as shown in Fig. 11 and results of fitting are presented in Table 5.

The microstructure of all the samples show the coatings to be dense and pore free. Coatings are crystalline with a particle size of nearly 12–15 nm. The total stack thickness of $BaTiO_3/MgF_2/BaTiO_3$ when heat treated in a belt furnace was found to be 400 nm. There is a change in coating thickness for $BaTiO_3$ from first to third layer due to variation in surface wetting behavior. The first layer of $BaTiO_3$ was applied on glass substrate. But when the 3rd $BaTiO_3$ layer was applied, it was deposited on MgF_2. Moreover, the first $BaTiO_3$ applied on glass exhibited uniform refractive index values throughout the wavelength range as against the top most $BaTiO_3$. In the belt furnace it may be noted that the first layer undergoes three heat treatments, whereas the top most layer undergoes only one heat treatment cycle. The consistency in the results obtained were also verified by generating three numbers of samples at the optimized parameters of coating and heat treatment in a belt furnace. The obtained results are presented in the following Fig. 12.

The corresponding average transmittance values over the visible and NIR wavelength range for the bare and solar control coated glass are presented in Table 6.

A comparison of the optical properties of the $BaTiO_3/MgF_2/BaTiO_3$ stack with that of the TiO_2/zeolite/TiO_2 stack as reported in [6] is presented in Table 7.

It can be seen that though the NIR blocking properties are the same for both the stacks, the visible light transmittance is considerably high in the case of the $BaTiO_3/MgF_2/BaTiO_3$ stack. This aspect is very much desirable for the solar control coatings.

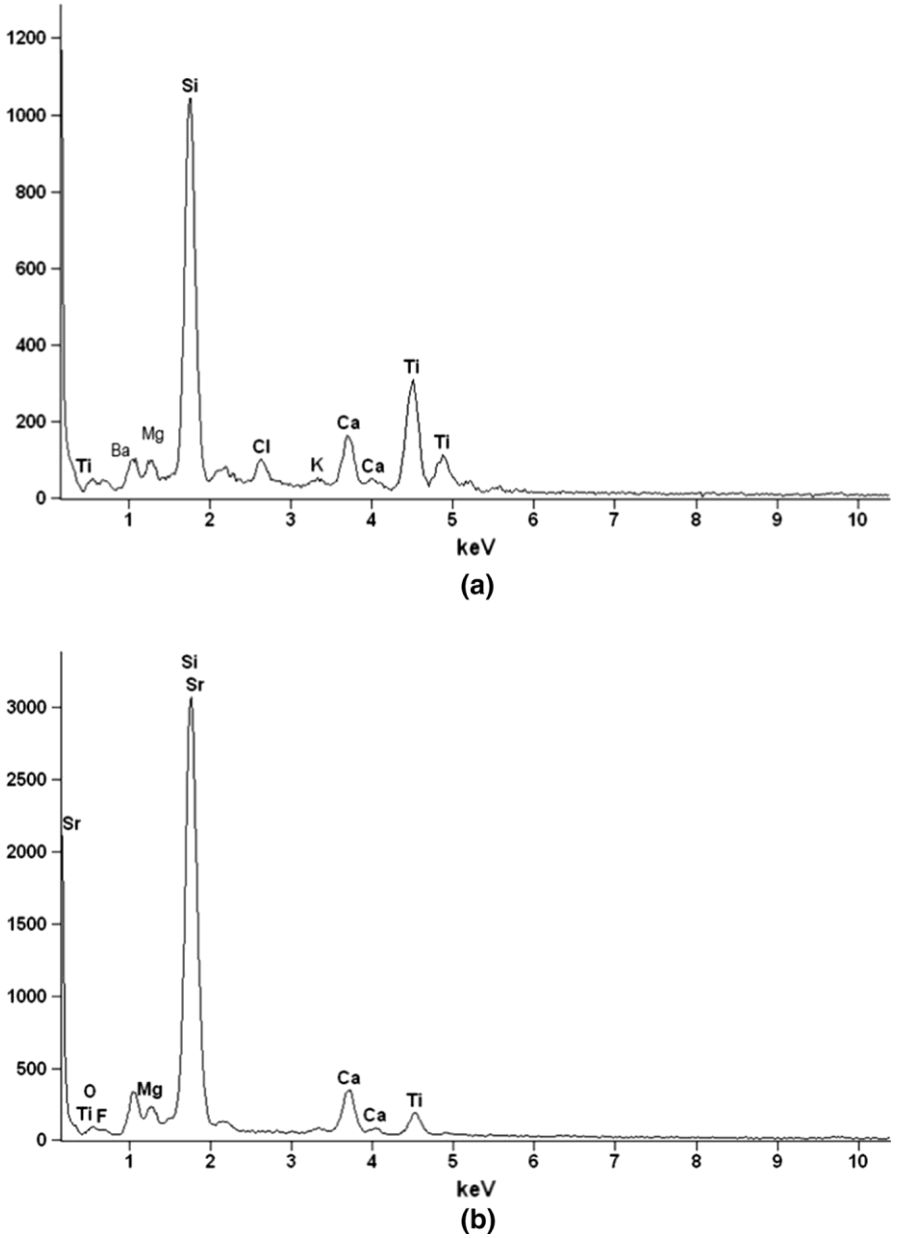

Fig. 7 EDAX pattern of **a** $BaTiO_3/MgF_2/BaTiO_3$ and **b** $SrTiO_3/MgF_2/SrTiO_3$ coatings applied on SLG and heat treated at 450 °C

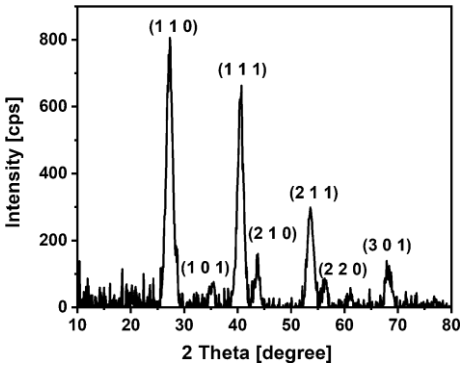

Fig. 8 XRD spectrum of MgF_2 powder after drying of MgF_2 sol after autoclaving

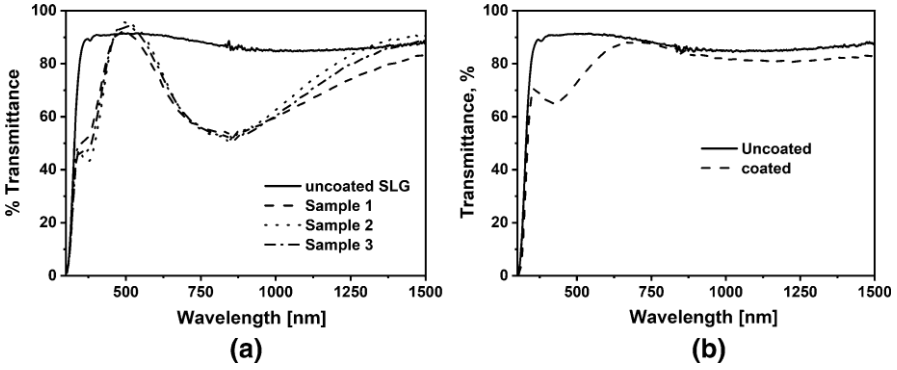

Fig. 9 Transmittance spectra for **a** $BaTiO_3/MgF_2/BaTiO_3$ and **b** $SrTiO_3/MgF_2/SrTiO_3$

Table 3 Transmittance data presented in percentage of bare and solar control coated glass with $BaTiO_3$ and $SrTiO_3$ as high refractive index materials in visible and NIR wave length ranges

Wavelength range (nm)	Bare glass	$BaTiO_3/MgF_2/BaTiO_3$	$SrTiO_3/MgF_2/SrTiO_3$
400–800	90.0	73.2	80.3
800–1500	85.7	68.0	80.2

Conclusions

$BaTiO_3/MgF_2/BaTiO_3$ and $SrTiO_3/MgF_2/SrTiO_3$ stacks with optimized thicknesses were generated on soda lime glass substrates and their solar control properties studied. Though both the stacks exhibit a NIR blocking effect, $BaTiO_3$-based stack performed better. In this case, it can be seen that there is > 30% reduction in the NIR transmittance of the glass while maintaining the visible light transmittance at > 65%. Such coatings show immense potential for the automotive and architectural applications to reduce the load on air conditioning. Moreover,

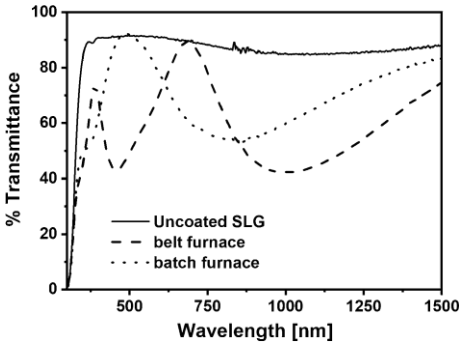

Fig. 10 Transmittance spectra as a function of annealing rates

Table 4 Transmittance data of bare and coated glass in visible and NIR wave length

Wavelength range (nm)	Bare glass	$BaTiO_3/MgF_2/BaTiO_3$ HT in belt furnace	$BaTiO_3/MgF_2/BaTiO_3$ HT in batch furnace
400–800	90	66.5	73.2
800–1500	85.7	55.4	68.0

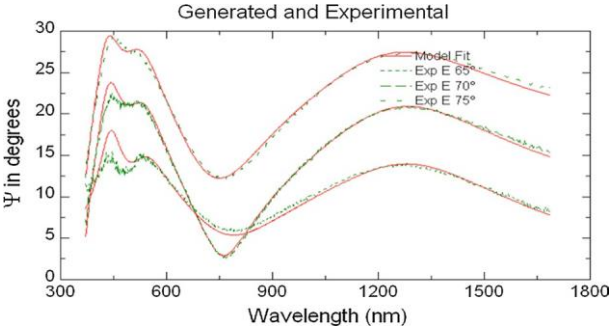

Fig. 11 Ellipsometer thickness profile of $BaTiO_3/MgF_2/BaTiO_3$ stack heat treated in belt furnace; $d_1 = 173$ nm; $d_2 = 74$ nm; $d_3 = 153$ nm and $n_1 = 1.82$; $n_2 = 1.40$; $n_3 = 1.90$ (at 550 nm)

Table 5 Refractive index values of each layer from $BaTiO_3/MgF_2/BaTiO_3$ stack heat treated in belt furnace

SLG sample with coating	Refractive index (n) at different wavelengths (nm)				Thickness (nm)
	550	800	1000	1300	
$BaTiO_3$—layer next to glass	1.82	1.82	1.82	1.82	173
MgF_2—middle layer	1.40	1.30	1.27	1.25	74
$BaTiO_3$—top most layer	1.90	1.86	1.85	1.84	153

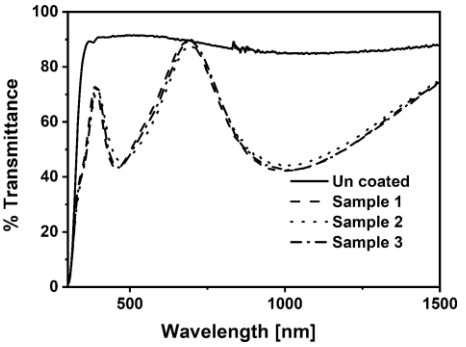

Fig. 12 Transmittance spectra of a batch of three coated samples with $BaTiO_3/MgF_2/BaTiO_3$ stack annealed at 450 °C in a belt furnace

Table 6 Average transmittance of uncoated and coated glass over visible and NIR wavelength range

Wavelength range (nm)	Average transmittance (%)			
Sample number	Bare glass	Sample 1	Sample 2	Sample 3
400–800	90.0	67.0	66.0	67.0
800–1500	86.0	54.0	55.0	54.0

Table 7 Comparison of transmittance values of $BaTiO_3/MgF_2/BaTiO_3$ with that of TiO_2/zeolite/TiO_2 stack

Stack/transmittance (%)	Visible light (400–800 nm)	NIR (800–1500 nm)
TiO_2/zeolite/TiO_2 [6]	38.0	54.0
$BaTiO_3/MgF_2/BaTiO_3$	67.5	54.0

the combination of $BaTiO_3$ as high refractive index material with MgF_2 as low refractive index material exhibits superior solar control properties with just a three-layer stack when compared to TiO_2 as high refractive index material and zeolite as low refractive index material. Further work is in progress to verify the durability of the coatings under service conditions.

Acknowledgements The authors acknowledge Director, International Advanced Research Centre for Powder Metallurgy and New Materials (ARCI), Hyderabad and Head of the Belarusian State University of Informatics and Radioelectronics (BSUIR), Minsk, Belarus for their constant support during the course of our investigation. Funding from the Department of Science and Technology, India and State Committee on Science and Technology of the Republic of Belarus under the India–Belarus bilateral joint cooperation through Grant Number INT/BLR/P-18/2016 (India) and Grant Number 17-001 (Belarus) is gratefully acknowledged.

References

1. M. Rydzek, M. Reidinger, S.M. Arduini, J. Manara, Thin Solid Films **520**, 4114 (2012)
2. V. Fang, J. Kennedy, J. Futter, J. Manning, GNS Sci. Rep. **39**, 1 (2013)

3. V.A. Maiorov, Opt. Spectrosc. **124**, 559 (2018)
4. L.M. Fortes, M.C. Goncalves, R.M. Almeida, Y. Castro, A. Duran, J. Non-Cryst. Solids **377**, 250 (2013)
5. Z. Nagamedianova, R.E. Ramírez-García, S.V. Flores-Arévalo, M. Miki-Yoshida, M. Arroyo-Ortega, Opt. Mater. **33**, 1999 (2011)
6. S. Manasa, R. Subasri, J. Coat. Technol. Res. **13**, 623 (2016)
7. J. Lott, C. Xia, L. Kosnosky, C. Weder, J. Shan, Adv. Mater. **20**, 3649 (2008)
8. F.M. Pontes, E.J.H. Lee, E.R. Leite, E. Longo, J. Mater. Sci. **35**, 4783 (2000)
9. G.J. Reynolds, M. Kratzer, M. Dubs, H. Felzer, R. Mamazza, Materials **5**, 644 (2012)
10. N. Serpone, Res. Chem. Intermed. **20**, 953 (1994)
11. M. Afshar, A. Badiei, H. Eskandarloo, G.M. Ziarani, Res. Chem. Intermed. **42**, 7269 (2016)
12. X. Li, G. Wang, Y. Cheng, Res. Chem. Intermed. **41**, 3031 (2015)
13. Y. Cao, K. Zhu, J. Du, J. Liu, J. Qiu, Res. Chem. Intermed. **41**, 4851 (2015)
14. D. Pasero, R.J.D. Tilley, Res. Chem. Intermed. **25**, 229 (1999)
15. S. Pavithra, R. Subasri, J. Coat. Sci Technol. **1**, 8 (2014)